

Beam energy dependence of the expansion dynamics in relativistic heavy ion collisions: Indications for the critical end point?

Roy A. Lacey

Depts. of Chemistry & Physics, Stony Brook University, NY 11974

Abstract

The flow harmonic v_n and the emission source radii R_{out} , R_{side} and R_{long} are studied for a broad range of centrality selections and beam collision energies in Au+Au ($\sqrt{s_{NN}} = 7.7 - 200$ GeV) and Pb+Pb ($\sqrt{s_{NN}} = 2.76$ TeV) collisions at RHIC and the LHC respectively. They validate the acoustic scaling patterns expected for hydrodynamic-like expansion over the entire range of beam energies studied. The combined data sets allow estimates for the $\sqrt{s_{NN}}$ dependence of the mean expansion speed $\langle c_s \rangle$, emission duration $\langle \Delta\tau \rangle$ and the viscous coefficients $\langle \beta'' \rangle$ that encode the magnitude of the specific shear viscosity $\langle \eta/s \rangle$. The estimates indicate initial-state model independent values of $\langle \eta/s \rangle$ which are larger for the plasma produced at 2.76 TeV (LHC) compared to that produced at 200 GeV (RHIC) ($\langle 4\pi\eta/s \rangle_{\text{LHC}} = 2.2 \pm 0.2$ and $\langle 4\pi\eta/s \rangle_{\text{RHIC}} = 1.3 \pm 0.2$). They also show a non-monotonic $\sqrt{s_{NN}}$ dependence for $\langle \beta'' \rangle$, $\langle c_s \rangle$ and $\langle \Delta\tau \rangle$, with minima for $\langle \beta'' \rangle$ and $\langle c_s \rangle$, and a complimentary maximum for $\langle \Delta\tau \rangle$. These dependencies signal a significant change in reaction dynamics in a narrow span of $\sqrt{s_{NN}}$, which may be linked to reaction trajectories close to the critical end point (CEP) in the phase diagram for nuclear matter.

Keywords:

1. Introduction

Heavy ion collisions provide an important avenue for studying the phase diagram for Quantum Chromodynamics (QCD) [1, 2, 3]. The location of the phase boundaries and the critical end point (CEP), in the plane of temperature vs. baryon chemical potential $[(T, \mu_B)\text{-plane}]$, are fundamental “landmarks” of this phase diagram [4]. Lattice QCD calculations suggest that the quark-hadron transition is a crossover at high T and small μ_B or high collision energies ($\sqrt{s_{NN}}$) [5]. Experimental results from the Relativistic Heavy Ion Collider (RHIC) at $\sqrt{s_{NN}} = 200$ GeV and the Large Hadron Collider (LHC) at $\sqrt{s_{NN}} = 2.76$ TeV, indicate that this transition results in the production of a strongly coupled plasma of de-confined quarks and gluons (sQGP) with low specific shear viscosity η/s , *i.e.* the ratio of shear viscosity η to entropy density s [6]. The validation of this crossover transition, which is a necessary, albeit insufficient, requirement for the existence of the CEP, serves as an important impetus for the ongoing experimental searches.

A current strategy for (i) establishing the essential “landmarks” of the phase diagram and (ii) pinning down the thermodynamic and transport properties of each QCD phase, is centered on measurements in energy scans designed to access the broadest possible (T, μ_B) -domain of the phase diagram. In this proceedings we follow this lead by leveraging the combined measurements for anisotropic flow and HBT radii, recently obtained by PHENIX and STAR in the first RHIC Beam Energy Scan (BES-I) and by ATLAS, ALICE and CMS at the LHC.

¹Roy.Lacey@Stonybrook.edu

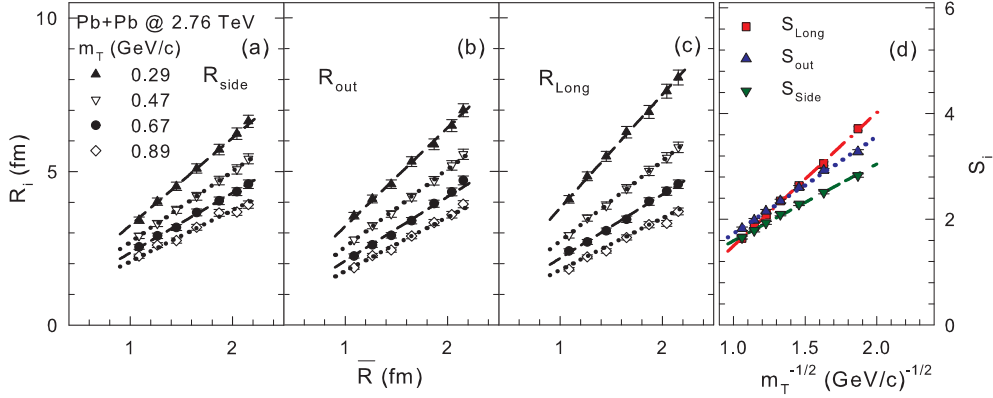


Figure 1. (Color online) HBT radii vs. \bar{R} for several m_T cuts (as indicated) for (a) R_{side} , (b) R_{out} and (c) R_{long} for Pb+Pb collisions at $\sqrt{s_{NN}}=2.76$ TeV; the data are taken from Ref. [17]. The dashed and dotted curves indicate linear fits to the data (see text). (d) S_i vs. $1/\sqrt{m_T}$; S_i are slopes obtained from the respective linear fits to the scaled values of R_{side} , R_{out} and R_{long} , shown in (a), (b) and (c). The dashed, dashed-dot and dotted curves in this panel, represent linear fits.

2. Probes for transport properties and the Critical End Point (CEP)

The expansion dynamics of relativistic heavy ion collisions is strongly influenced by the transport properties of the created medium, as well as the path of the reaction trajectory in the (T, μ_B) -plane. Such an influence can manifest as quantifiable changes in the magnitude of the space-time extent of the emission source, characterized by the so-called HBT radii R_{out} , R_{side} and R_{long} ; the square of (i) the emission source lifetime $\tau^2 \propto R_{\text{long}}^2$, (ii) its geometric size $R_{\text{geo}}^2 \propto R_{\text{side}}^2$ and (iii) the emission duration $\Delta\tau^2 \propto (R_{\text{out}}^2 - R_{\text{side}}^2)$ [7]. It can also manifest as a significant modulation of the anisotropic flow coefficients v_n , depending on the magnitude of η/s . The LHC measurements at $\sqrt{s_{NN}} = 2.76$ TeV, allow investigations of the space-time extent and η/s at high T and small μ_B ; they complement similar measurements from BES-I which allow a systematic study for the μ_B and T values spanned by the collision energy range $\sqrt{s_{NN}} = 7.7\text{--}200$ GeV. Here, it is noteworthy that currently, there are only a few experimental constraints for the (T, μ_B) -dependence of η/s , especially at the lower beam energies [8].

At the CEP or close to it, anomalies in the dynamic properties of the medium can drive abrupt changes in transport coefficients and relaxation rates to give a non-monotonic dependence of $\frac{\eta}{s}(T, \mu_B)$ [6, 9, 10]. An emitting system produced in the vicinity of the CEP is also expected to show a stalling of the expansion speed and a larger emission duration manifested as a difference between R_{out} and R_{side} ($\Delta\tau^2 \propto (R_{\text{out}}^2 - R_{\text{side}}^2)$) [11]. Here, the rationale is that, in the vicinity of the CEP, the equation of state (EOS) “softens” considerably and this slows down the speed of expansion and prolongs the emission duration to give $R_{\text{out}} > R_{\text{side}}$.

In prior work [12, 13], we have used the participant eccentricities (ε_n) and initial transverse size \bar{R} ($1/\bar{R} = \sqrt{(1/\sigma_x^2 + 1/\sigma_y^2)}$, where σ_x and σ_y are the respective root-mean-square widths of the density distributions) obtained with Monte Carlo Glauber (MC-Glauber) simulations, to validate the acoustic nature of the expansion dynamics [14] in RHIC and LHC collisions. This acoustic property predicts a linear relationship between the expansion time (t) and the initial transverse size ($t \propto \bar{R}$), as well as a characteristic linear dependence of $\ln(v_n/\varepsilon_n)$ on both n^2 and $1/\bar{R}$, with slopes $\beta' \propto (\eta/s)$ and $\beta'' \propto (\eta/s)$. We use the latter scaling patterns in conjunction with viscous hydrodynamical calculations [15, 16], to calibrate β' and β'' and make estimates of $\langle\eta/s\rangle$ for the plasma produced in Au+Au and Pb+Pb collisions at 200 GeV and 2.76 TeV respectively. A further study of the $\sqrt{s_{NN}}$ dependence of β'' , c_s and $\Delta\tau$ is then used to search for non-monotonic patterns which could signal the presence of the CEP.

3. Results

Representative summaries of the the scaling properties of the HBT radii and v_n are shown in Figs. 1 and 2 respectively. Figs. 1(a), (b) and (c) validate the expected linear dependence of R_{side} , R_{out} and R_{long} on \bar{R} . They also show the expected decrease in the slope of the respective scaling curves (for R_{side} , R_{out} and R_{long}) with increasing transverse mass m_T . The latter confirms the important influence of the space-momentum correlations which result

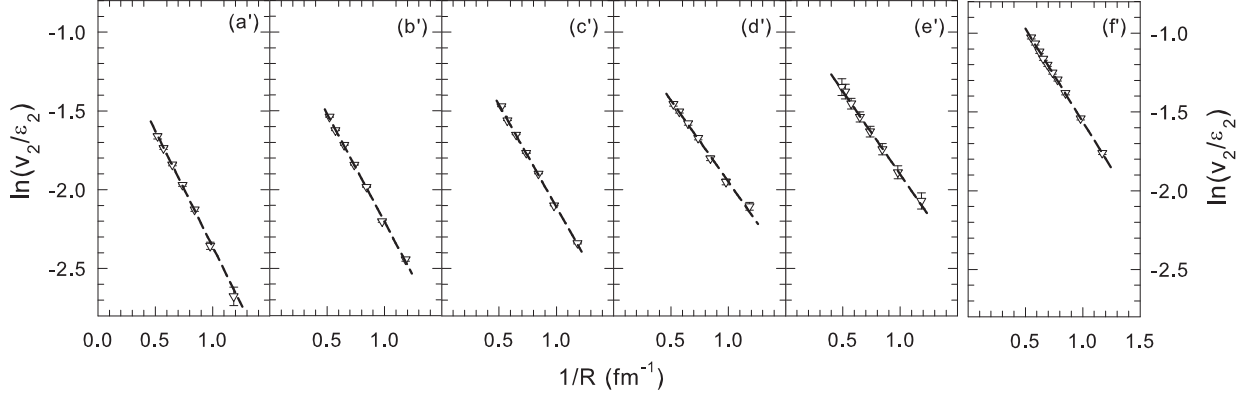


Figure 2. ((a') – (e')) $\ln(v_2/\varepsilon_2)$ vs. $1/\bar{R}$ for p_T -integrated v_2 ($p_T \gtrsim 0.2$ GeV/c) for Au+Au collisions. (f') $\ln(v_2/\varepsilon_2)$ vs. $1/\bar{R}$ for p_T -integrated v_2 ($p_T = 0.3 - 3$ GeV/c) for Pb+Pb collisions. The data for Au+Au and Pb+Pb collisions are taken from Refs. [18, 19] and Ref. [20] respectively. The dashed curves represent linear fits to the data; error bars are statistical only.

from collective expansion. Fig. 1(d) shows that the slopes S_i , obtained from linear fits (dashed and dotted curves) to the data in panels (a)-(c), scale as $1/\sqrt{m_T}$ and the space-momentum correlations are largest (smallest) in the long (side) direction. They also indicate that, for a given $\sqrt{s_{NN}}$, the full set of differential measurements (as a function of centrality and m_T) for each radius, can be made to scale to a single curve. Similar scaling patterns were observed for the full range of $\sqrt{s_{NN}}$ values spanned by the PHENIX and STAR data sets.

Figures 2(a') – (f') show the expected linear dependence of $\ln(v_n/\varepsilon_n)$ vs. $1/\bar{R}$ for the full range of available beam energies. This pervasive pattern of scaling provides the basis for a consistent method of extraction of the viscous coefficient $\beta'' \propto \eta/s$, via linear fits to the scaled data for each beam energy. The characteristic linear dependence of $\ln(v_n/\varepsilon_n)$ on both n^2 and $1/\bar{R}$, with slopes $\beta' \propto (\eta/s)$ and $\beta'' \propto (\eta/s)$ was also observed for viscous hydrodynamical calculations [21]. Consequently, such calculations were used to calibrate β' and β'' and extract η/s for the plasma produced in Au+Au and Pb+Pb collisions at 200 GeV (RHIC) and 2.76 TeV (LHC) respectively. This procedure give the values $\langle 4\pi\eta/s \rangle_{\text{RHIC}} = 1.3 \pm 0.2$ and $\langle 4\pi\eta/s \rangle_{\text{LHC}} = 2.2 \pm 0.2$ which are insensitive to the initial-state geometry model employed [21].

The results from a search for possible non-monotonic patterns linked to the CEP, are summarized in Figs. 3 and 4. The $\sqrt{s_{NN}}$ dependence for β'' (Fig. 3) shows a decreasing trend from 7.7 GeV to approximately 62.4 GeV, followed by a relatively slow increase from $\sqrt{s_{NN}} = 62.4$ GeV - 2.76 TeV. Here, it should be emphasized that the error bars for the extractions made at 62.4, 130 and 200 GeV, as well as a lack of measurements between 39 and 62.4 GeV, do not allow a definitive estimate of the precise location of this apparent minimum. Nonetheless, we associate this characteristic $\sqrt{s_{NN}}$ dependence of β'' with the expected trend of $\frac{\eta}{s}(T, \mu_B)$ for reaction trajectories in the vicinity of the CEP [9, 10]. If this is so, such trajectories should also lead to signatures indicative of a softening of the EOS and a prolonged emission duration. The results from the tests for such signatures are shown in Fig. 4.

The $\sqrt{s_{NN}}$ dependence of $(R_{\text{out}}^2 - R_{\text{side}}^2) \propto \Delta\tau^2$ and $(R_{\text{side}} - \sqrt{2}\bar{R})/R_{\text{long}}$ are shown in Figs. 4 (a) and (b) respectively. $(R_{\text{side}} - \sqrt{2}\bar{R})/R_{\text{long}}$ is used as a proxy for the expansion speed c_s since $(R_{\text{side}} - \sqrt{2}\bar{R})$ represent the expansion radius and $R_{\text{long}} \propto \tau$. Fig. 4 shows the anticipated non-monotonic trends; they indicate a maximum for $\langle \Delta\tau \rangle$ and a complimentary minimum for $\langle c_s \rangle$ in the same narrow span of $\sqrt{s_{NN}}$. These dependencies signal a significant change in reaction dynamics which could also be linked to reaction trajectories close to the CEP.

4. Conclusions

In summary, we have presented a detailed study of the expansion dynamics in relativistic heavy ion collisions, using the combined data sets for flow and HBT measurements in Pb+Pb collisions at $\sqrt{s_{NN}} = 2.76$ TeV and Au+Au collisions spanning $\sqrt{s_{NN}} = 7.7 - 200$ GeV. Our study shows that the scaling properties of these measurements validate the characteristic signatures expected for sound propagation in the matter produced in these collisions. They also allow estimates for the $\sqrt{s_{NN}}$ dependence of the mean expansion speed $\langle c_s \rangle$, emission duration $\langle \Delta\tau \rangle$ and the

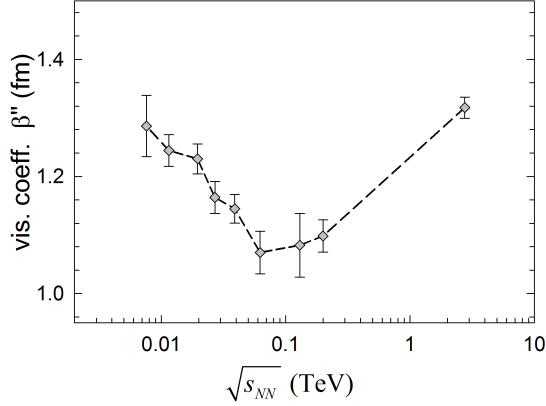


Figure 3. Viscous coefficient β'' vs. $\sqrt{s_{NN}}$, extracted from linear fits to $\ln(v_2/\varepsilon_2)$ vs. $1/\bar{R}$; error bars are statistical only. The dashed curve is drawn to guide the eye.

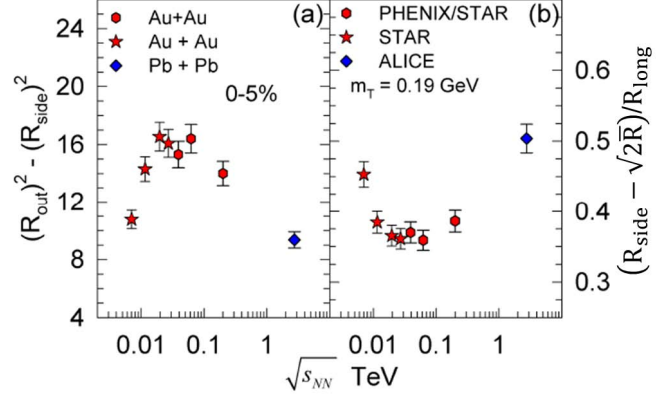


Figure 4. (Color online) $\sqrt{s_{NN}}$ dependence of (a) $(R_{out}^2 - R_{side}^2) \propto \Delta\tau^2$, (b) $[(R_{side} - \sqrt{2}R)/R_{long}] \propto \langle c_s \rangle$. The HBT radii used for these extractions are taken from preliminary PHENIX data and Refs. [17, 22].

viscous coefficients $\langle\beta''\rangle$ that encode the magnitude of the specific shear viscosity $\langle\eta/s\rangle$. The estimates indicate a larger value of $\langle\eta/s\rangle$ for the plasma produced at 2.76 TeV (LHC) compared to that produced at 200 GeV (RHIC) ($\langle 4\pi\eta/s \rangle_{\text{LHC}} = 2.2 \pm 0.2$ and $\langle 4\pi\eta/s \rangle_{\text{RHIC}} = 1.3 \pm 0.2$); these values are insensitive to the choice of the initial-state model employed for the extractions. They also show a non-monotonic $\sqrt{s_{NN}}$ dependence for $\langle\beta''\rangle$, $\langle c_s \rangle$ and $\langle\Delta\tau\rangle$, with minima for $\langle\beta''\rangle$ and $\langle c_s \rangle$, and a complimentary maximum for $\langle\Delta\tau\rangle$. These dependencies signal an important change in the reaction dynamics for a narrow range of $\sqrt{s_{NN}}$, which may be linked to reaction trajectories close to the critical end point. Further detailed studies, with improved errors and modeling, are required to make a more precise mapping, as well as to confirm if the observed patterns for $\langle\beta''\rangle$, $\langle c_s \rangle$ and $\langle\Delta\tau\rangle$, are definitively linked to decay trajectories close to the critical end point in the phase diagram for nuclear matter.

Acknowledgments

This research is supported by the US DOE under contract DE-FG02-87ER40331.A008.

References

- [1] N. Itoh, Prog. Theor. Phys. 44 (1970) 291–292.
- [2] E. V. Shuryak, CERN-83-01, CERN-YELLOW-83-01.
- [3] M. A. Stephanov, K. Rajagopal, E. V. Shuryak, Phys.Rev.Lett. 81 (1998) 4816–4819, doi:10.1103/PhysRevLett.81.4816.
- [4] M. Sasaki, K. Yazaki, Nucl. Phys. A 504 (1989) 668.
- [5] Y. Aoki, G. Endrodi, Z. Fodor, S. Katz, K. Szabo, Nature 443 (2006) 675–678, doi:10.1038/nature05120.
- [6] R. A. Lacey, et al., Phys. Rev. Lett. 98 (2007) 092301, doi:10.1103/PhysRevLett.98.092301.
- [7] S. Chapman, P. Scotto, U. W. Heinz, Phys.Rev.Lett. 74 (1995) 4400–4403, doi:10.1103/PhysRevLett.74.4400.
- [8] R. A. Lacey, A. Taranenko, J. Jia, D. Reynolds, N. Ajitanand, et al., Phys.Rev.Lett. 112 (2014) 082302, doi:10.1103/PhysRevLett.112.082302.
- [9] L. P. Csernai, J. Kapusta, L. D. McLerran, Phys.Rev.Lett. 97 (2006) 152303, doi:10.1103/PhysRevLett.97.152303.
- [10] R. A. Lacey, N. Ajitanand, J. Alexander, P. Chung, J. Jia, et al., arXiv:0708.3512.
- [11] D. H. Rischke, M. Gyulassy, Nucl.Phys. A608 (1996) 479–512, doi:10.1016/0375-9474(96)00259-X.
- [12] R. A. Lacey, Y. Gu, X. Gong, D. Reynolds, N. Ajitanand, et al., arXiv:1301.0165.
- [13] R. A. Lacey, A. Taranenko, N. Ajitanand, J. Alexander, arXiv:1105.3782.
- [14] P. Staig, E. Shuryak, Phys.Rev. C84 (2011) 034908, doi:10.1103/PhysRevC.84.034908.
- [15] H. Song, S. A. Bass, U. Heinz, T. Hirano, C. Shen, Phys.Rev. C83 (2011) 054910, doi:10.1103/PhysRevC.83.054910, 10.1103/PhysRevC.86.059903.
- [16] See Fig. 14 in CMS PAS HIN-12-011., ???
- [17] A. Kisiel, PoS WPCF2011 (2011) 003.
- [18] L. Adamczyk, et al., Phys.Rev. C86 (2012) 054908, doi:10.1103/PhysRevC.86.054908.
- [19] G. Agakishiev, et al., Phys.Rev. C86 (2012) 014904, doi:10.1103/PhysRevC.86.014904.
- [20] S. Chatrchyan, et al., Phys.Rev. C87 (2013) 014902, doi:10.1103/PhysRevC.87.014902.
- [21] R. A. Lacey, D. Reynolds, A. Taranenko, N. Ajitanand, J. Alexander, et al., arXiv:1311.1728.
- [22] L. Adamczyk, et al., arXiv:1403.4972.